Hindawi
Advances in Materials Science and Engineering
Volume 2022, Article ID 1956040, 14 pages
https://doi.org/10.1155/2022/1956040

Research Article

Effect of Carbon Fiber Admixture and Length on Microwave Deicing Efficiency of Airport Road Surface Concrete

Yi-peng Ning,[1] **Jin-yu Xu**,[1,2] **He Huang**,[1] **Zhi-hang Wang**,[1] **and Ao Yao**[1]

[1]*Department of Airfield and Building Engineering, Air Force Engineering University, Xi'an 710038, China*
[2]*College of Mechanics and Civil Architecture, Northwest Polytechnic University, Xi'an 710072, China*

Correspondence should be addressed to Yi-peng Ning; ningyipeng1998@163.com

Received 9 May 2022; Accepted 25 May 2022; Published 9 June 2022

Academic Editor: Samson Jerold Samuel Chelladurai

In order to improve the microwave deicing efficiency of airport road surface concrete, the method of incorporating carbon fiber materials of different doping amounts and lengths into concrete is proposed. The test method is optimized by using a fiber-optic temperature sensor and a self-developed open microwave deicing vehicle, and the effect of the coupling effect of different carbon fiber doping and length on the microwave deicing efficiency of concrete is studied. The results of the study show that the appropriate amount of carbon fiber blended into the concrete can significantly improve the microwave deicing efficiency, and the reasonable use of carbon fiber-modified concrete can achieve the purpose of efficient deicing of the airport road surface. By analyzing the temperature rise curve, temperature rise rate curve, deicing effect, and infrared thermography of the microwave deicing process, combined with the "heat generation-heat dissipation" theory, the microwave deicing is divided into four stages: concrete wave absorption, water layer formation, ice thinning, and ice breaking and ice melting. In the process of microwave deicing of concrete, changing the length of carbon fiber and the amount of doping will have a greater impact on the rate of temperature rise and deicing range, but the shape of deicing remains basically the same, mainly spindle-shaped. When the length of carbon fiber is short, it is not conducive to the absorption of microwave by concrete, and with the increase of fiber length and doping amount, the wave absorption performance of carbon fiber-modified concrete on the airport road surface is gradually improved; when the fiber length is 0.6 cm and the fiber doping amount is 2‰, the wave absorption performance is the best, and the deicing rate is 1.82 times of ordinary concrete, and the deicing area is 1.2 times of ordinary concrete.

1. Introduction

Airport is an important infrastructure to guarantee aircraft take-off, landing, taxiing, and parking, and airport road surface is an important part of the airport. The normal use of airport road surface requires not only sufficient strength, but also good flatness and suitable roughness. NASA reports that 35% of aircraft accidents are related to road surface friction and that a road surface friction coefficient of less than 0.2 is dangerous. Studies have shown that the friction coefficient of new cement concrete pavement is 0.82, while the snow and ice pavement is only 0.15. Snow and ice on the road surface will greatly reduce the friction coefficient of the road surface, and if the road surface ice is not cleared effectively in time [1], aircraft take-off and landing are likely to experience handling failure and brake skid, reducing efficiency and even causing safety accidents [2, 3]. Currently, the commonly used deicing methods are mechanical deicing, chemical deicing, and thermal deicing [4, 5]. Chemical deicing corrodes the road surface, pollutes the environment, and costs more; mechanical deicing easily damages the road surface and has a low removal rate; and thermal deicing consumes serious energy, takes a long time to heat, and the temperature of the road surface after heating is high and unevenly distributed, which is more likely to cause damage to the road surface. Microwave deicing, as a new deicing technology [6–9], is a low-energy consumption, fast heating speed, and pollution-free deicing method, which has received wide attention from scholars worldwide. Microwave deicing has the advantages of no damage to the road surface, high

removal rate, economic and environmental protection, etc. Its principle is to irradiate microwaves on the icing surface, using the selectivity of microwave heating, through the ice surface directly to the road surface, to destroy the adhesion between the ice surface and the concrete road surface and finally achieve the effect of removing the ice layer of the concrete road surface. However, its deicing efficiency for traditional concrete road surface is low [10], which is not easy to promote the use. Therefore, how to effectively improve the efficiency of microwave deicing for road surface has become a hot spot for research at home and abroad. In 2013, Gallego [11] added 10-mm long steel fibers with a mass doping of 0.2% to asphalt concrete and used microwave irradiation for 120 s. The results showed that the surface temperature of the specimen could reach more than 140°C. In 2017, Liu et al. [12] studied the effect of different amounts of graphite on the microwave deicing efficiency of concrete. The results showed that the addition of graphite significantly improved the microwave deicing efficiency. When the content of graphite is 15%, the heating rate is 2.5 times that of ordinary concrete, and the effective deicing area is 2.2 times that of ordinary concrete. The time of effective deicing area is shortened by 40 seconds. In 2018, Liu et al. [13–17] found that the incorporation of iron black into concrete can improve the deicing efficiency and a greater range of deicing, and the microwave heating efficiency was increased by 192% at 15% admixture, but the incorporation of iron black reduced the mechanical properties of concrete. In 2019, Wang et al. [18] prepared microwave heated aggregate (MHA) from magnetite and replaced the original aggregate. Compared with ordinary pavement, the addition of MHA greatly improved the deicing performance of deicing pavement; the deicing time of MHA100 at −20°C and −5°C decreased by 56.0% and 54.8%, respectively.

Carbon fiber, which contains more than 90% carbon, is a high-modulus, high-strength fiber with good electrical conductivity and has good durability, thermal conductivity, and corrosion resistance [19–22]. Carbon fiber cement matrix composites can absorb microwaves well and reflect less than −10 dB under low-frequency (less than 8 GHz) electromagnetic wave irradiation [23, 24], in addition, carbon fiber has good toughness and high tensile strength, which can effectively enhance the strength of concrete and improve the related performance defects. At present, microwave deicing research at home and abroad is focused on carbon fiber-modified asphalt concrete [22, 25, 26], and there is still a gap in the study of carbon fiber-modified cement concrete, and a systematic study of the performance of cement concrete in absorbing microwave heating and deicing is needed.

In conclusion, microwave deicing technology with its special heating principle has its unique advantages among many deicing methods and technologies and is favored by many scholars at home and abroad. The microwave irradiation in this article adopts a self-developed highly adjustable microwave deicing equipment, and a fiber-optic sensor is used to measure the surface temperature change law of the specimen to avoid large measurement errors of the metal sensor due to microwave irradiation. This article takes carbon fiber-modified concrete as the research object and studies the effect of different carbon fiber admixture and length on microwave deicing efficiency of airport road surface.

2. Experiment

2.1. Experiment Material. The cement in this article is 42.5 R grade ordinary silicate cement produced by Shaanxi Yaobai Cement Factory, the fine aggregate is natural sand of Weihe River, and the coarse aggregate is limestone crushed stone produced by the hammer crusher, which is divided into small stone (5~10 mm), medium stone (10~20 mm), and large stone (20~40 mm), and the ratio of small stone:medium stone:large stone is 0.5 : 1 : 1; the mixing water is used to supply the water of Lianhu District, Xi'an City. As shown in Figure 1, the lengths of carbon fiber were 0.1 cm, 0.3 cm, and 0.6 cm, respectively, considering that the length of carbon fiber was not easy to be evenly dispersed in the concrete aggregate when the length of carbon fiber exceeded 6 mm. Each technical index is shown in Table 1.

2.2. Specimen Preparation

(1) After the concrete specimens are prepared according to the ratio shown in Table 2, the fabricated foam molds are placed on the wire mesh on the ground, keeping the bottom of the molds horizontal. The center point T_0 and edge point T_1 are marked on the surface of the specimen to locate the fiber-optic sensors for later deployment. The specimen was then placed into the mold, and the gap between the specimen and the mold was filled with foam, where the center point T_0 was located at the center of the whole specimen surface and the edge point T_1 was positioned with the center point T_0 as the reference and displaced by 5 cm in the lateral and longitudinal directions.

(2) The two fiber-optic temperature sensors are placed at predetermined positions inside the refrigeration cabinet, and then the specimen is added to the cabinet. The test water is slowly poured into the mold until the water layer covers the upper surface of the concrete specimen, and the height of the corner of the refrigeration cabinet is adjusted so that the water layer on the surface of the specimen is evenly distributed, where the thickness is consistent everywhere.

(3) The test water is injected continuously in the mold, while placing a centimeter scale inside the mold to control the thickness of the water layer, and the process is stopped when the thickness of the water layer reaches 1 cm. Finally, the test piece was frozen in the refrigeration cabinet for 8 h and then taken out. The effect of the test piece ice layer preparation is shown in Figure 2.

(a) (b) (c)

Figure 1: Different lengths of carbon fiber. (a) 0.1 cm, (b) 0.3 cm, and (c) 0.6 cm.

Table 1: Main technical specifications of carbon fiber.

Project	Length			Diameter	Tensile strength	Modulus	Density
Company		cm		μm	GPa	GPa	kg/L
Numerical value	0.1	0.3	0.6	8	3.1	23	1.62

Table 2: Carbon fiber-modified airport road surface concrete ratio design.

Grouping	Cement	Water	Sand	Stone	Water reducer	Carbon fiber		
						Dosage 1‰	Dosage 2‰	Dosage 3‰
Quality/kg	320	140	592	1377	3.52	1.62	3.24	4.86

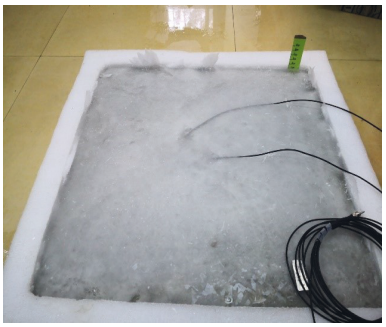

Figure 2: Ice layer preparation.

Figure 3: Magnetron.

2.3. Experiment Apparatus and Equipment

2.3.1. The Selection of Magnetron. This article uses a magnetron to excite the microwave, the magnetron model OM75P (31) ESGN, the microwave power emitted is 1000 W, and the frequency is 2.45 GHz (Figure 3).

2.3.2. The Selection of Waveguide Port. The waveguide port used in this article is the BJ-22 waveguide port produced by Shanghai Saihan Machinery Co (Figure 4), and the internal section size is 109.2 mm × 54.6 mm.

2.3.3. Independent Design of Open Adjustable Height Microwave Deicing Equipment. Open microwave deicing technology was used in the test. Unlike microwave ovens and other closed microwave deicing devices, the open adjustable height microwave deicing equipment (Figure 5) was designed independently and commissioned by Shanghai Saihan Machinery Equipment Co. Microwave deicing vehicle height can be modified by four corners, but multi-microwave source heating and multi-microwave source relative position can be adjusted by the horizontal adjustment lever, emulating genuine engineering deicing conditions.

2.3.4. Fiber-Optic Temperature Sensor. In order to prevent microwave interference with the temperature measurement sensor, the test uses fiber-optic temperature sensor for temperature measurement. Fiber-optic sensor is YL-PL type passive fiber-optic temperature sensor (Figure 6) and is used

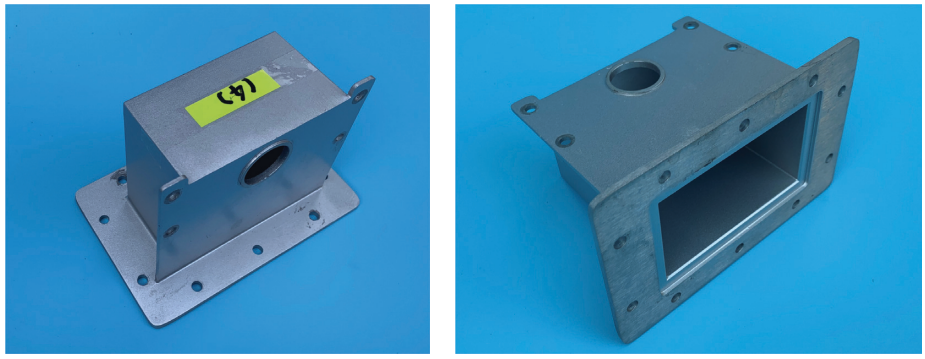

(a) (b)

Figure 4: Waveguide port.

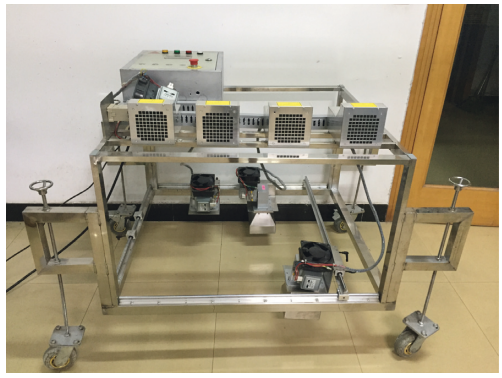

Figure 5: Open adjustable height multi-wavelength source microwave deicing vehicle.

Figure 6: Fiber-optic temperature sensor.

to measure the temperature of a fixed point on the upper surface of the concrete specimen. In addition, a paperless recorder is used to store the temperature data (Figure 7).

2.3.5. Infrared Imager. FLIR ONE PRO infrared imager is used for infrared temperature recording, the temperature range is −20°C~400°C, the thermal sensitivity is 150 mK, and the thermal information of the object surface is obtained through noncontact thermal imaging. The thermal resolution of the infrared imager is 120 × 160, and the accuracy is ±3°C. The infrared thermal imaging map records the

Figure 7: Paperless recorder.

Table 3: Grouping table of carbon fiber concrete specimens.

Length (cm)	Dosage (‰)			
	0	1	2	3
0.1	PC	—	—	0.1CFC3
0.3		—	—	0.3CFC3
0.6		0.6CFC1	0.6CFC2	0.6CFC3

temperature value of 307200 points on the surface of the specimen, which is convenient to accurately grasp the surface temperature distribution of the specimen.

2.4. Experiment Scheme and Procedure. The specimens were grouped as shown in Table 3 according to the length of the doped carbon fiber and the amount of doping.

In order to explore the feasibility of carbon fiber-modified concrete used for microwave deicing of road surface, the following steps were followed in the experimental study of carbon fiber-modified concrete microwave deicing efficiency change law and deicing mechanism.

In this article, six groups of specimens with different length and content of carbon fiber were subjected to microwave deicing test with ice layer, which was irradiated by an open microwave deicing vehicle. First, the specimen with ice layer is heated by microwave irradiation for 120 s. At the same time, the temperature rise curves of central point T_0

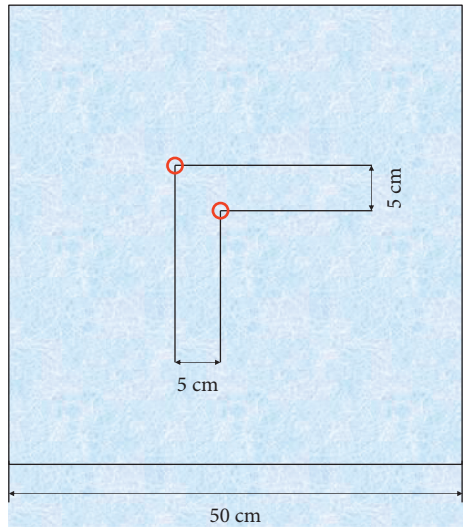

Figure 8: Schematic diagram of temperature measurement center point T_0 and edge point T_1.

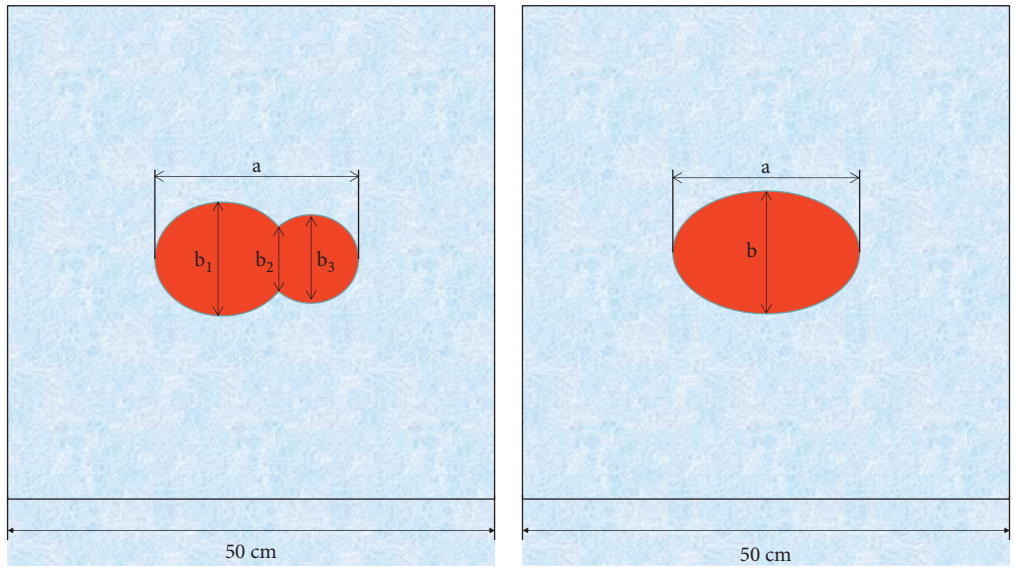

(a) (b)

Figure 9: Schematic diagram of the shape of the deicing area. (a) Spindle-shaped deicing area. (b) Oval deicing area.

and edge point T_1 are measured by optical fiber sensor and paperless recorder, and the data points are recorded. The relative positions of T_0 and T_1 are shown in Figure 8. The deicing effect picture and infrared thermal imaging picture are taken after microwave heating [22] of 120 s. Finally, the melting form of the ice layer is observed, and the melting area and shape information of the ice layer are recorded. Figure 9 is a schematic diagram of the deicing area. When the deicing area is spindle-shaped, the shape characteristics of the deicing area are represented by the length of the symmetry axis a, the length of the center line b_2, and the widths b_1 and b_3 of the left and right semicircles (Figure 9(a)). When the deicing area is oval, the shape characteristics of the deicing area are represented by the lengths a and b of two symmetry axes (Figure 9(b)).

3. Results and Discussion

3.1. Effect of Carbon Fiber Length on Microwave Deicing Efficiency. In order to study the effect of carbon fiber length on the microwave deicing efficiency of road surface concrete, four groups of specimens with different fiber lengths (PC, 0.1CFC3, 0.3CFC3, and 0.6CFC3) were tested for microwave irradiation with ice layer, and PC specimens were taken as the control group.

3.1.1. Effect of Carbon Fiber Length on Temperature Rise Rate. Figure 10 shows the temperature rise curves under the carbon fiber lengths of 0.1 cm, 0.3 cm, and 0.6 cm when the carbon fiber doping is 3‰, Figure 11 shows the effect of

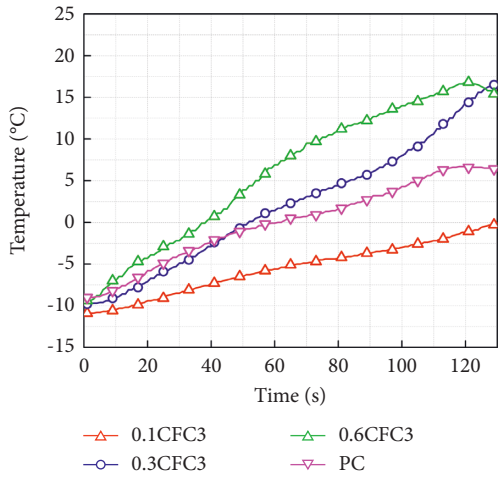

Figure 10: Comparison of temperature rise curves at different lengths.

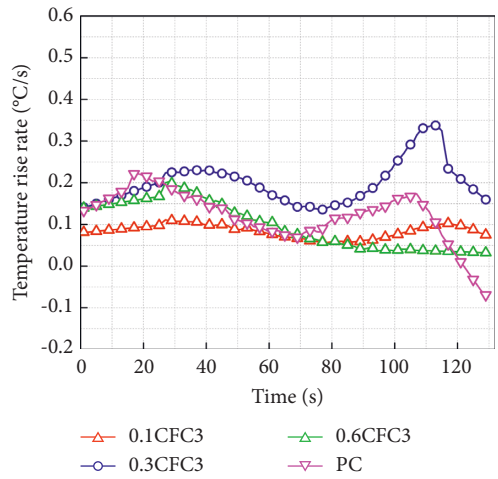

Figure 11: Comparison of temperature rise rate curves at different lengths.

different carbon fiber lengths on the temperature rise rate, and Figure 12 shows the effect of different carbon fiber lengths on the deicing effect. From the figures, it can be seen that:

(1) The doping amount is constant, and the temperature rise [27] decreases first and then increases with the increase of carbon fiber length. When the length of carbon fiber is 0.6 cm, the temperature rise of the specimen is the highest, up to 26.2°C, and the microwave deicing effect is the best. (2) When the carbon fiber doping amount was 3‰, the temperature rise amplitude increased with the increase of carbon fiber length, in which the temperature rise amplitude of 0.6CFC3 was about 2.7 times of 0.1CFC3. (3) The temperature rise curve of PC specimen with the increase of microwave irradiation time is on the rise, and the temperature rise rate curve in the first 20 s appeared in the peak, 0.22°C/s. The temperature rise rate then decreases, which is due to the PC specimen's surface temperature rise after wave absorption, causing the temperature difference between the ice layers to expand further. In the case of unchanged heat production efficiency, heat dissipation efficiency rises, resulting in a lower temperature rise rate. When the microwave irradiation time is 60 s, the surface temperature of the PC specimen rises to 0°C, when the ice layer begins to melt to generate liquid water. Water has good wave absorption properties, which in turn leads to increased heat production efficiency and increases the temperature rise rate. When the microwave irradiation time reaches 108 s, the temperature rise rate curve appears obvious decreasing section. This is due to the water layer has been basically formed and covered the surface of the test piece, the basic heat production efficiency remains unchanged, the thickness of the ice layer before breaking sharply reduced; when the thickness of the ice layer tends to 0, the temperature difference tends to infinity, so the heat dissipation efficiency increases sharply and the rate of temperature rise significantly reduced. However, the duration of this stage is short, and the temperature rise amplitude does not change much, and thus coincides with the smaller deicing area in the deicing area table. (4) Temperature rise rate curve showed an inflection point at 112 s, indicating that at this point the rate of heat dissipation increased sharply, the rate of heat production remained stable, the ice layer absorbed a large amount of heat until melting, the phenomenon of ice breakage occurred, the deicing effect was schematic, and it was fully consistent. (5) 0.1CFC3 temperature rise curve of the temperature rise is very small, only 9.7°C, the temperature of the center point T_0 is always lower than 0°C, the temperature rise rate [28] changes with time is small, only about 0.1°C/s, which indicates that the 0.1CFC3 test piece of wave absorption and deicing performance is poor. (6) When the temperature reaches 0°C, the peak of the temperature rise rate curve of 0.3CFC3 specimen is larger than the previous section, which indicates that the deicing effect is better than the PC group, the ice layer melts water area is larger, the wave absorption and heat generation efficiency is higher, and the deicing area table further verifies the analysis conclusion. (7) The overall temperature rise curve of the 0.6CFC3 specimen is located above 0.3CFC3, but its overall temperature rise rate curve resides below 0.3CFC3. When the surface center point temperature T_0 of the specimen reaches 0°C before, the temperature rise rate can be up to 0.2°C/s. (8) When the surface center temperature T0 of the 0.6CFC3 specimen reached 0 °C, the temperature rise rate curve began to rise, but after a short time, an inflection point occurred, and the temperature rise rate began to decline; at this point, the thickness of the ice layer decreased, and the water layer had essentially formed. (9) The temperature rise rate curve fluctuates against 0.3CFC3 at the time of 100s, and it is initially determined that the ice breaking phenomenon occurs at this time, which then triggers the temperature rise rate fluctuation, and the main reason is that the heat dissipation rate at the time of ice breaking produces a precipitous fall, so the temperature rise rate curve rises, but with the continuous depth of ice breaking, the ice breaking area further expands.

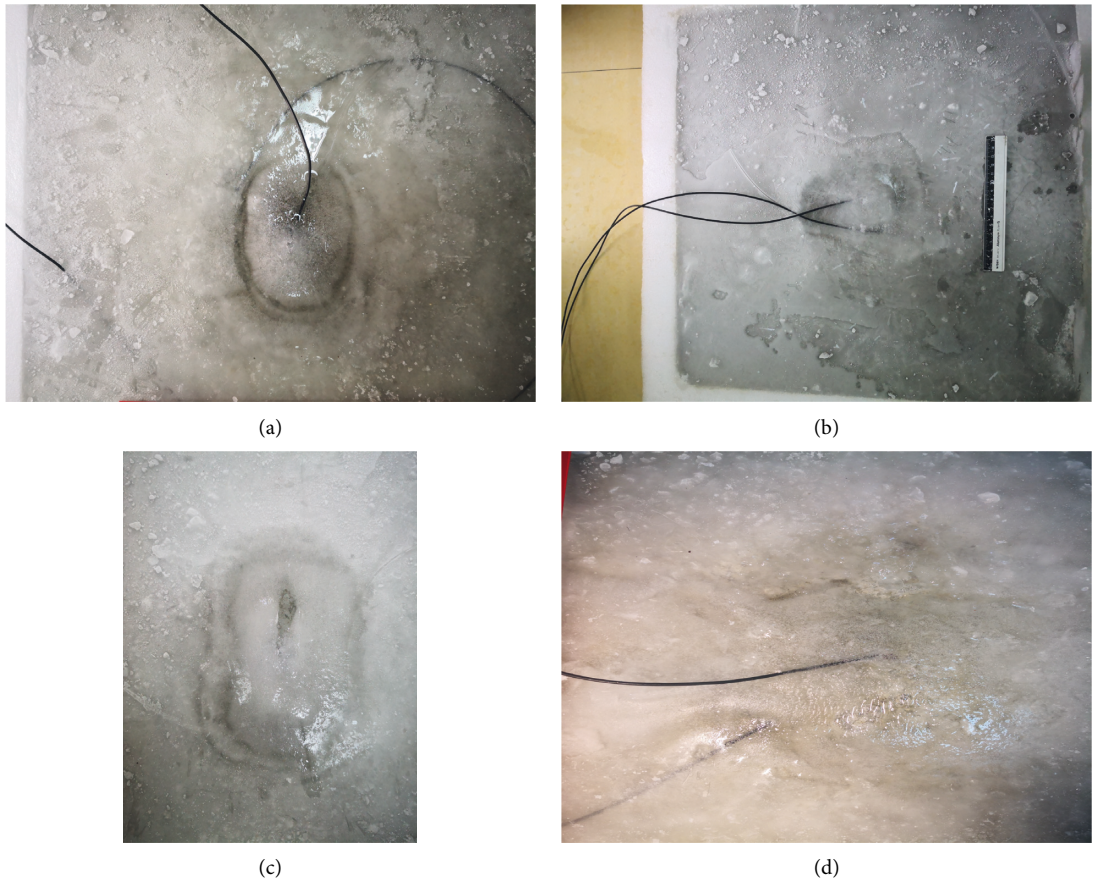

(a) (b) (c) (d)

Figure 12: Deicing effect diagram under different lengths. (a) PC. (b) 0.1CFC3. (c) 0.3CFC3. (d) 0.6CFC3.

3.1.2. Effect of Carbon Fiber Length on Deicing Range. Figure 13 shows the 3D stereogram of surface temperature of the specimens with different carbon fiber lengths and the infrared thermogram, which together with Table 4 reflects the effect of carbon fiber length on the deicing area and deicing shape, from which it can be obtained that:

(1) The final deicing area of the PC specimen is 125.59 cm^2, and the shape of the deicing area is basically the same as that in the infrared thermogram, which is spindle-shaped, indicating that the infrared thermogram can reflect the shape and size of the deicing area. (2) The actual deicing area of 0.1CFC3 is only 22.10 cm^2, and there is no ice-breaking phenomenon on the upper surface of the ice layer. Combined with the infrared thermogram, the overall color is dark, indicating that the actual heating area is small. (3) In the deicing treatment of the ice layer with a hammer, only a small hole can be broken out of the ice, indicating that the ice layer and the concrete surface have not yet separated, resulting in low deicing efficiency and poor results. (4) The actual deicing area of 0.3CFC3 specimen is 149.12 cm^2, which is much larger than 0.1CFC3. (5) From the 3D stereogram of the surface of 0.3CFC3 specimen, it can be seen that there is an obvious temperature spike on the surface of the specimen, which corresponds to the red dot area in the infrared thermogram, thus judging that the ice-breaking phenomenon has occurred here. The sudden temperature change is due to the good wave absorption performance of the water layer and the high efficiency of heat production. (6) 0.6CFC3 deicing area of 163.73 cm^2 is about 1.3 times the PC. 0.6CFC3 infrared imaging map does not appear in the red area, the surface temperature of the test piece 3D stereo map as a whole is relatively flat, indicating that the temperature difference within the entire microwave deicing area is small, and the uniformity of microwave heating is good.

3.2. Effect of Carbon Fiber Doping on Microwave Deicing Efficiency. In order to study the effect of carbon fiber doping on the microwave deicing efficiency of road surface concrete, four groups of specimens with different fiber doping (PC, 0.6CFC1, 0.6CFC2, and 0.6CFC3) were tested with microwave irradiation of ice layer, and PC specimens were taken as the control group.

3.2.1. Effect of Carbon Fiber Doping on the Rate of Temperature Rise. Figure 14 shows the temperature rise curves under the carbon fiber length of 1‰, 2‰, and 3‰ when the carbon fiber length is 0.6 cm, Figure 15 shows the effect of different carbon fiber doping on the temperature rise rate, and Figure 16 shows the effect of different carbon fiber doping on the deicing effect. From the figures, it can be seen that:

(1) The length is constant, and the temperature rise increases first and then decreases with the increase of carbon

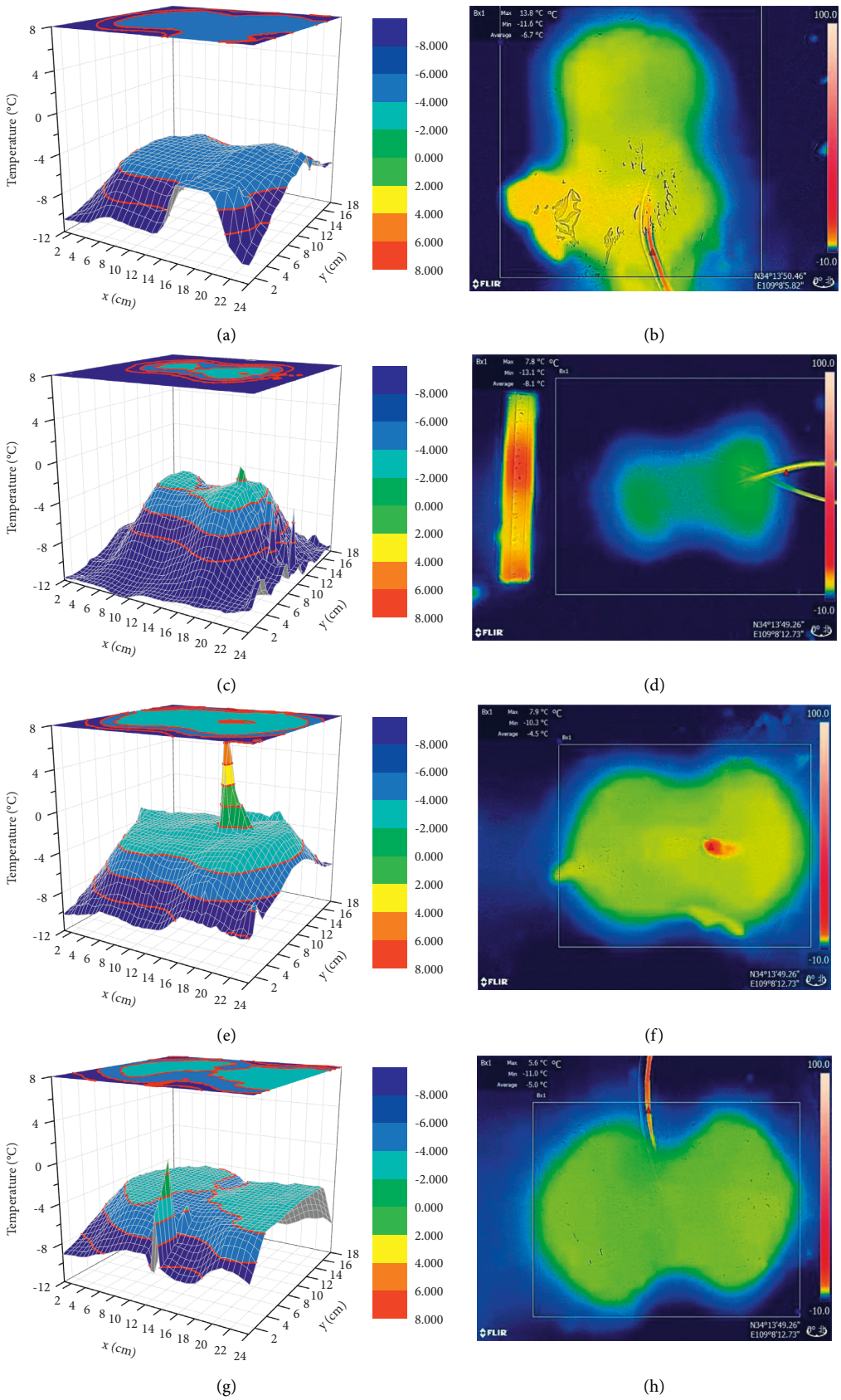

FIGURE 13: 3D stereogram and IR thermogram of surface temperature at different lengths. (a) PC-1. (b) PC-2. (c) 0.1CFC3-1. (d) 0.1CFC3-2. (e) 0.3CFC3-1. (f) 0.3CFC3-2. (g) 0.6CFC3-1. (h) 0.6CFC3-2.

Table 4: Deicing area at different lengths.

Parameter	Test piece			
	PC	0.1CFC3	0.3CFC3	0.6CFC3
Shape	Spindle shape	Ellipse	Spindle shape	Spindle shape
S_c/cm^2	125.59	22.10	149.12	163.73
a/cm	15.38	7.14	16.97	18.22
$b_1(b)$/cm	9.19	3.74	10.10	11.28
b_2/cm	8.49	—	7.50	7.45
b_3/cm	9.15	—	10.51	11.00

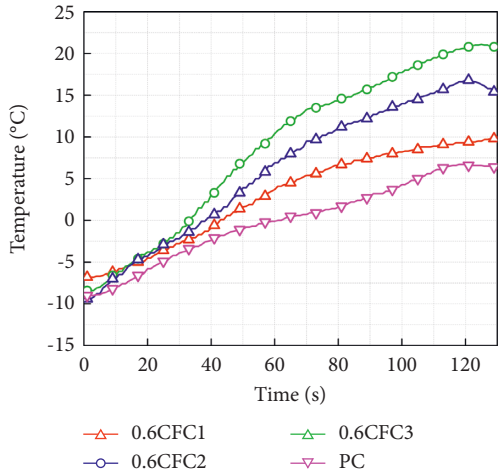

Figure 14: Comparison of temperature rise curves at different doping levels.

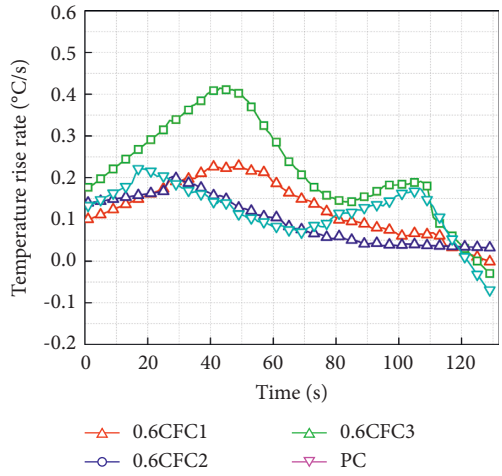

Figure 15: Comparison of temperature rise rate curves under different doping amounts.

fiber doping. When the carbon fiber doping amount is 2‰, the temperature rise of the specimen is the highest, up to 29°C, and the microwave deicing effect is the best. (2) When the length of carbon fiber is 0.6 cm, with the increase of carbon fiber doping, the temperature rise amplitude increases first and then decreases, in which the temperature rise amplitude of 0.6CFC2 is about 1.8 times of 0.6CFC1. (3) The temperature rise of 0.6CFC1 is 15.8°C, which is close to that of PC. 0.6CFC1 has a peak temperature rise rate of 0.23°C/s, which is only half of that of 0.6CFC2, and the temperature rise rate curve before 40 s has a rising trend and the overall change is not large. (4) When the time is 50 s, the temperature rise rate curve appears inflection point, indicating that the water layer is basically formed at this time, due to the reduction of the thickness of the ice layer leads to the rate of heat dissipation exceeds the rate of heat production, the temperature rise rate curve begins to appear a decreasing section. (5) The temperature rise of 0.6CFC2 is 29°C, which is 1.84 times of the temperature rise of 0.6CFC1, and the peak of the temperature rise rate curve is as high as 0.42°C/s. (6) When 0.6CFC2 surface center point temperature T0 reaches 0°C before the temperature rise rate curve does not appear to fall section, which is mainly the 0.6CFC2 heat production rate double the PC, the center point T0 temperature reaches 0°C twice as fast as the PC; before the emergence of the water layer, the thickness of the ice layer is certain, and the heat dissipation rate has not exceeded the heat production rate, so the temperature rise rate has a rising trend. (7) When the time is 33 s, the water layer begins to appear; because the water absorption efficiency is higher than the ice layer, the heat production rate increases, further increasing the temperature rise rate. The temperature rise rate curve appears at the inflection point at 44 s, which indicates that due to the reduction in ice layer thickness, heat dissipation rate exceeds heat production rate, and the temperature rise rate curve begins to descend, at which point the water layer is basically formed. (8) After the formation of the early water layer, it directly leads to the transverse temperature conduction is much larger than the longitudinal temperature conduction, and the deicing area increases continuously but the deicing depth increases slowly, as shown by the temperature rise rate curve and the deicing effect graph, the ice-breaking phenomenon only starts to appear at 83 s and the area is small. (9) The temperature rise of 0.6CFC3 is 26.2°C, which is 1.67 times of the temperature rise of 0.6CFC1, and the maximum temperature rise rate is 0.2°C/s. (10) Before the temperature T_0 at the center of 0.6CFC3 surface reaches 0°C, the temperature rise rate curve is relatively flat compared with the other three curves, and the temperature rise rate tends to a stable value. (11) When the surface center temperature T_0 of 0.6CFC3 reaches 0°C, the temperature rise rate curve shows an increasing trend, but after a short time, there is an inflection point and the temperature rise rate starts to decrease, when the ice

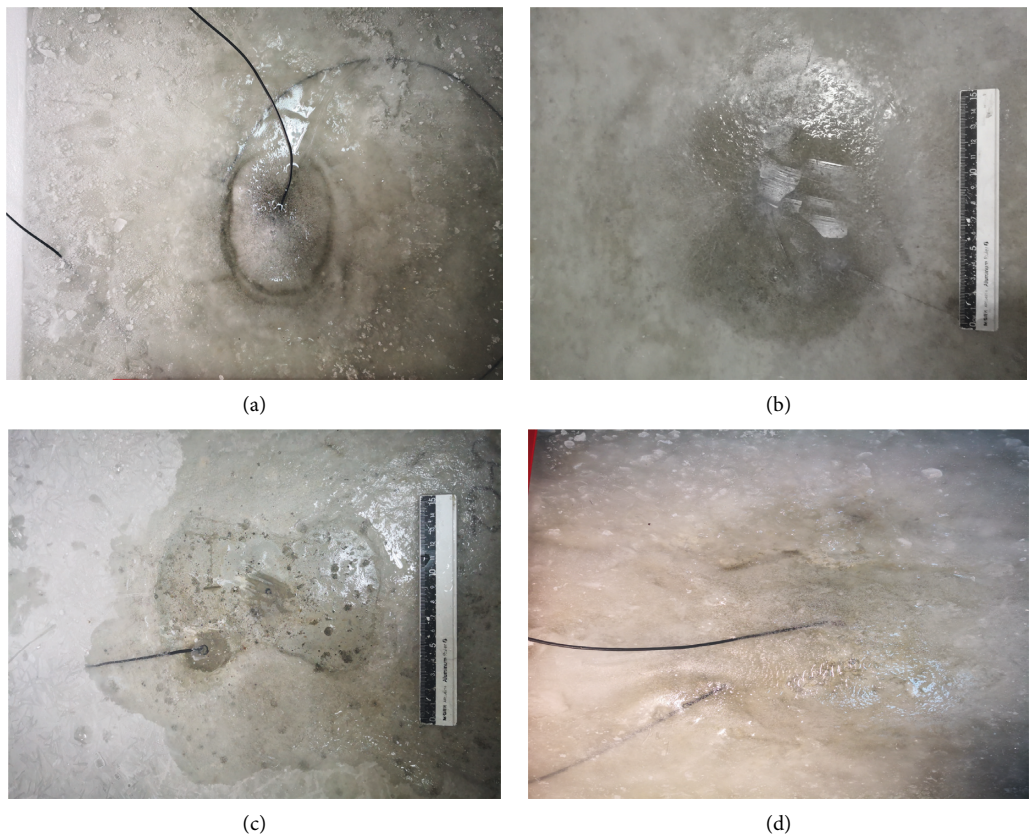

(a) (b) (c) (d)

Figure 16: Deicing effect at different dosing levels. (a) PC. (b) 0.6CFC1. (c) 0.6CFC2. (d) 0.6CFC3.

thickness decreases and the water layer has basically formed. (12) The temperature rise rate curve for 0.6CFC3 fluctuates in the 100s, compared to 0.6CFC2. It is initially determined that the phenomenon of ice breaking occurs at this time, which in turn triggers the temperature rise rate fluctuation. The main reason is that the heat dissipation rate at the moment of ice breaking produces a precipitous fall, so the temperature rise rate curve rises. However, when the ice-breaking progresses, the ice-breaking area grows even more, the heat dissipation rate gradually exceeds the heat generation rate, and the temperature increase rate curve drops once more. The temperature rise rate curve decreases again as the ice-breaking area expands further, and the heat dissipation rate gradually exceeds the heat production rate.

3.2.2. Effect of Carbon Fiber Doping on Deicing Range. Figure 17 shows the 3D stereogram of surface temperature and infrared thermogram of specimens with different carbon fiber lengths, which together with Table 5 reflect the effect of carbon fiber doping on the deicing area and deicing shape, from which it can be obtained that:

(1) The deicing efficiency of 0.6CFC1 specimen is not significantly improved, and the final deicing area is 137.82 cm^2, which is only 1.1 times of PC. (2) From the 3D stereogram of the surface of the 0.6CFC1 specimen, it can be seen that there is an obvious temperature spike on the surface of the specimen, which corresponds to the red dot area in the infrared thermogram, and the ice-breaking phenomenon is judged to occur here. The sudden temperature change is due to the good wave absorption performance of the water layer and the high efficiency of heat production. (3) Although the 0.6CFC2 specimen has poor ice-breaking effect, the deicing area is larger, and the final deicing area is 149.21 cm^2, which is about 1.2 times of PC. (4) The infrared thermographic image of 0.6CFC2 shows a red dotted area, and it is judged that there is a sudden temperature change peak point here, and combined with the 3D stereogram of the surface temperature of the specimen, it is inferred that this is the ice-breaking area. (5) The deicing area of 0.6CFC3 is 163.73 cm^2, about 1.2 times that of 0.6CFC2. 0.6CFC3 surface temperature 3D stereogram is relatively gentle overall, slightly raised spikes, the surface temperature of −2~−4°C area is roughly spindle-shaped, combined with infrared thermography analysis shows that the temperature difference between the entire microwave deicing area of each region does not vary significantly.

Let τ_0 be the moment when the concrete surface temperature reaches 0°C, τ_1 be the moment when the water layer is completely formed, $\Delta\tau$ be the time from the complete formation of the water layer to the breaking of the ice, the deicing area is S_c, and the temperature rise is T_f. In order to

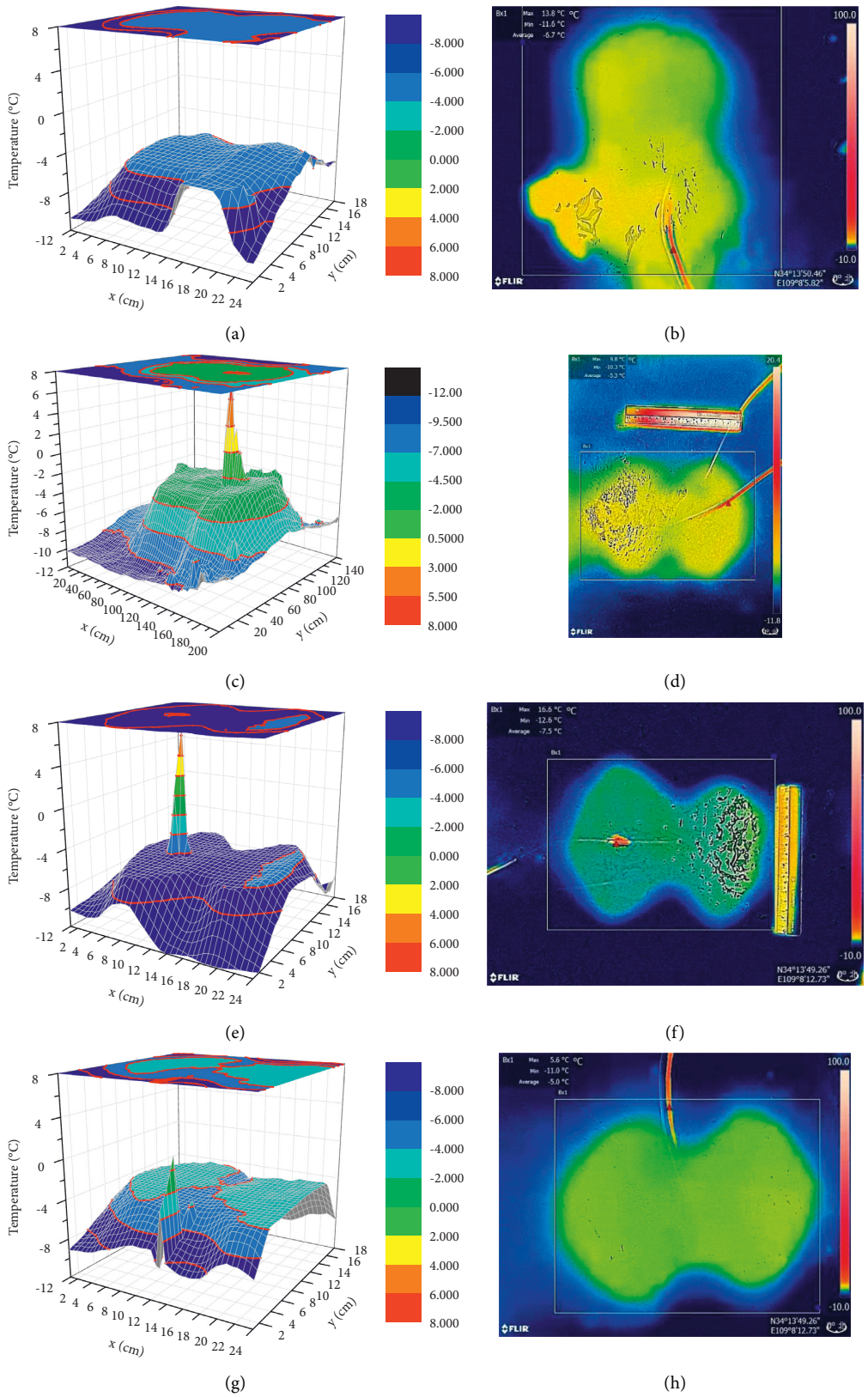

Figure 17: 3D stereogram and IR thermogram of surface temperature at different doping levels. (a) PC-1. (b) PC-2. (c) 0.6CFC1-1. (d) 0.6CFC1-2. (e) 0.6CFC2-1. (f) 0.6CFC2-2. (g) 0.6CFC3-1. (h) 0.6CFC3-2.

Table 5: Deicing area at different dosing levels.

Parameter	Test specimen			
	PC	0.6CFC1	0.6CFC2	0.6CFC3
Shape	Spindle	Spindle	Spindle	Spindle
S_c/cm^2	125.59	137.82	149.21	163.73
a/cm	15.38	18.71	16.80	18.22
$b_1(b)$/cm	9.19	11.49	10.67	11.28
b_2/cm	8.49	6.72	7.55	7.45
b_3/cm	9.15	10.81	10.92	11.00

Table 6: Comparison of microwave deicing efficiency with different carbon fiber doping and length.

Projects	τ_0	τ_1	$\Delta\tau$	S_c	T_f
Unit	s	s	s	cm^2	˚C
PC	60	116	—	125.59	16.8
0.1CFC3	—	—	—	22.10	9.7
0.3CFC3	52	112	8	149.12	24.2
0.6CFC2	33	44	38	149.21	29
0.6CFC3	38	51	42	163.73	26.2

make a more intuitive comparison of the deicing efficiency of different specimens, statistics were conducted for the above five indicators, as shown in Table 6.

4. Mechanistic Analysis

Microwaves, as a kind of electromagnetic wave [29, 30], are refracted, reflected, and projected after irradiation on the surface of an object, and dipoles are generated by the electric field they carry acting inside the medium, and the dipoles rub against each other and vibrate at high frequencies, converting the energy of the electromagnetic field [31–33] into internal energy. Therefore, the concrete surface is irradiated by microwaves and the concrete temperature increases. Since concrete is an insulator and carbon fiber is a conductor with good electrical conductivity, adding a certain length and doping amount of carbon fiber to concrete can significantly improve its electromagnetic properties, which in turn increases the temperature rise rate of concrete specimens and improves microwave deicing efficiency.

According to the chronological order, the microwave deicing process of carbon fiber concrete can be divided into four stages: concrete wave absorption stage, water layer formation stage, ice thinning stage, and ice breaking and ice melting stage. For any point in space, the rate of temperature rise is equal to the rate of heat production minus the rate of heat dissipation at that point, that is

$$\frac{\partial T_s}{\partial \tau} = \frac{\lambda}{c\rho}\nabla^2 T_s + \frac{0.566 \times 10^{-10}}{c\rho} f \varepsilon''_{\text{eff}} E^2_{rms}. \tag{1}$$

From equation (1), it can be seen that the temperature rise rate is affected by many factors, including thermal conductivity λ, specific heat capacity c, medium density ρ, frequency f, temperature T_s.

As the length of carbon fiber increases, the temperature rise rate of carbon fiber-modified concrete increases. This is due to the fact that changing the length of carbon fiber can change the electromagnetic parameters, and according to equation (2), as the length of carbon fiber increases, the path of electron polarization becomes longer, which in turn makes the overall dielectric constant of carbon fiber-modified concrete larger, increasing the efficiency of wave absorption and heat generation, and therefore the temperature rise rate increases, which is consistent with the experimental results.

$$(\varepsilon - \varepsilon_0)E = P = \lim_{\Delta v \longrightarrow 0} \frac{\sum ql}{\Delta v}. \tag{2}$$

With the increase of carbon fiber admixture, the temperature rise rate of carbon fiber-modified concrete increases first and then decreases. This is due to the fact that the modified dielectric constant imaginary part of carbon fiber-modified concrete is affected by many factors, including the electrical conductivity of the medium σ and the circular frequency of electromagnetic waves ω. According to equation (3), the conductivity of carbon fiber is greater than that of concrete, and the overall conductivity increases after adding carbon fiber, which, combined with equation (1), enhances the wave absorption and heat generation properties of concrete, and the temperature rise rate of concrete increases. Therefore, in the case of the same length, increasing the amount of carbon fiber in a certain range can improve the temperature rise rate, and thus improve the efficiency of microwave deicing. However, if the doping amount is too large, the carbon fibers become agglomerated and form a lapped closed loop to shield electromagnetic waves, which weakens the efficiency of microwave deicing.

$$\varepsilon''_{\text{eff}} = \varepsilon'' + \frac{\sigma}{\omega\varepsilon_0}. \tag{3}$$

Changing the fiber length and the amount of doping on the microwave deicing temperature rise rate, and the deicing area will also change, but the shape of the deicing is basically the same. In the case of constant heating time of 120 s, the change of length and doping amount will lead to the change of deicing area, mainly because its change will lead to the change of temperature rise rate. However, due to the constant shape and height of the flare, the deicing shape is basically unchanged, but different deicing efficiencies lead to different sizes of deicing area after the same deicing time, mainly spindle-shaped, with the two centers as the central point of heating and radiating in all directions.

On the whole, 0.6CFC2 has high temperature rise amplitude, fast temperature rise rate, and large deicing area and small ice-breaking area, and its deicing speed is 2.0 times, and deicing area is 1.2 times of ordinary concrete, compared with other specimens; 0.6CFC2 has the best deicing effect. Continue to increase the amount or length of carbon fiber doping on this basis will lead to the phenomenon of carbon fiber lap inside the concrete over a large area, forming a closed loop of electrical conductivity, and the microwave is reflected by a large number of concrete that cannot be

absorbed, resulting in microwave deicing efficiency instead of reducing.

5. Conclusion

In this article, we conducted an experimental study on the influence law of different carbon fiber lengths and doping amounts on the microwave deicing efficiency of road surface concrete and analyzed the mechanism of the temperature rise curve and temperature rise rate curve of microwave deicing by combining the deicing effect map and infrared thermography map for reference. The following are the main conclusions:

(1) According to the time sequence of microwave deicing, the temperature rise curve of deicing can be divided into four stages: concrete wave absorption stage, water layer formation stage, ice thinning stage, and ice breaking and ice melting stage; ice thickness and wave absorption medium are the main factors to determine the temperature rise rate, in which the heat dissipation rate will tend to infinity as the ice breaking progresses, so the temperature rise rate curve of ice breaking stage will increase and decrease cyclically. After the liquid water replaces the concrete as the wave-absorbing medium, the heat production rate increases, which in turn leads to an increase in the temperature rise rate.

(2) In the process of microwave deicing of concrete, changing the length and dosing of carbon fiber will have a large impact on the temperature rise rate and deicing range, but the shape of deicing remains basically the same.

(3) Compared with increasing the amount of carbon fiber, increasing the length of carbon fiber can improve the wave absorption performance of carbon fiber-modified concrete on the airport road surface. When the fiber length is long, too much increase in carbon fiber doping will reduce the wave absorption performance of the specimen, and there exists an optimal value of carbon fiber doping and length. In a certain range of carbon fiber admixture of 2‰ and length of 0.6 cm, the improvement effect is the best, the temperature rise rate is up to 0.42°C/s, which is 2 times higher than PC, the deicing time is 33~44 s, which is only 0.55 times of PC time, and the deicing area is 149.21 cm^2, which is 1.2 times higher than PC, meeting the deicing requirements in actual construction.

(4) The research in this article shows that the incorporation of carbon fiber in concrete can effectively improve the microwave deicing efficiency of concrete, and the research results will lay the foundation for the application and promotion of microwave deicing technology for airport road surface concrete. However, the factors affecting the efficiency of microwave deicing include microwave power, microwave frequency, waveguide height, external environmental temperature, and humidity. In order to make the microwave deicing technology to be effectively promoted and applied, these influencing factors will be the focus of our subsequent research.

Data Availability

Some data used to support the findings of this study are included within the article. And another data used to support the findings of this study are available from the corresponding author upon reasonable request.

Conflicts of Interest

The authors declare no conflicts of interest.

Acknowledgments

The authors express their thanks to all members of the laboratory team for their help and technical support. This research was funded by the National Natural Science Foundation of China and Youth Talent Promotion Program of Shaanxi University Association for Science and Technology under Grant nos. 51908548 and 20200415.

References

[1] X. Li, Y. Xu, and F. Liu, "Research on microwave deicing method," *Journal of Harbin Institute of Technology*, vol. 11, pp. 1342-1343, 2003.

[2] N. Q. Dong, "The current situation, dilemma and countermeasures of general aviation development in China," *Journal of Beijing University of Technology*, vol. 16, no. 01, pp. 110–117, 2014.

[3] Y. R. Xu, "Analysis of the impact of winter road maintenance on traffic safety," Dissertation, Southeast University, Nanjing, China, 2015.

[4] W. B. Yu, S. Y. Li, W. J. Feng, and X. Yi, "Current status of road snow and ice removal technology and its impact on traffic safety. Analysis of the current situation and development trend of road snow melting and deicing technology," *Glacial Permafrost*, vol. 33, no. 04, pp. 933–940, 2011.

[5] H. Y. Liu and P. W. Hao, "Road deicing technology and its development trend," *Road construction machinery and construction mechanization*, vol. 11, pp. 18–21, 2008.

[6] Z. Y. Wang, *Fundamentals of Microwave Technology*, p. 11, Beijing University Press, Beijing, China, 2003.

[7] Y. Zhang, W. H. Hao, and J. H. Gao, *Microwave Technology and Applications*, Xi'an University of Electronic Science and Technology Press, Xi'an, China, 2006.

[8] D. D. Guo and A. M. Sha, "Snow and ice melting technology based on the coupled heating effect of microwave and magnet," *Journal of Shandong University*, vol. 42, no. 04, pp. 92–97, 2012.

[9] C. G. Liao, D. Z. Chen, and L. J. Xue, *Fundamentals of Microwave Technology*, National Defense Industry Press, Beijing, China, 1979.

[10] G. W. Flintsch, *Assessment of the Performance of Several Roadway Mixes under Rain, Snow, and winter Maintenance Activities*, Virginia Center for Transportation Innovation and Research, China, 2004.

[11] J. Gallego, M. A. del Val, V. Contreras, and A. Páez, "Heating asphalt mixtures with microwaves to promote self-healing," *Construction and Building Materials*, vol. 42, pp. 1–4, 2013.

[12] J.-l. Liu, J.-y. Xu, and S. Lu, "Investigations on microwave deicing effects on graphite-modified concrete," *RSC Advances*, vol. 7, no. 62, pp. 39237–39243, 2017.

[13] J. L. Liu, T. L. Yao, J. Y. Xu, and X. C. Lv, "Study on the effect of iron black admixture on microwave deicing efficiency of concrete," *Concrete*, vol. 08, pp. 31–34, 2018.

[14] S. Lu, J. Xu, E. Bai, J. Liu, and X. Luo, "Investigating microwave deicing efficiency in concrete pavement," *RSC Advances*, vol. 7, no. 15, pp. 9152–9159, 2017.

[15] J.-L. Liu, J.-Y. Xu, S. Lu, and H. Chen, "Investigation on dielectric properties and microwave heating efficiencies of various concrete pavements during microwave deicing," *Construction and Building Materials*, vol. 225, pp. 55–66, 2019.

[16] H. Huang and J. Y. Xu, "Effect of magnetite on concrete mechanics and microwave deicing performance," *IOP Conference Series: Earth and Environmental Science*, vol. 267, no. 4, Article ID 042019, 2019.

[17] Z. Wang, J. Gao, T. Ai, and P. Zhao, "Laboratory investigation on microwave deicing function of micro surfacing asphalt mixtures reinforced by carbon fiber," *Journal of Testing and Evaluation*, vol. 42, no. 2, pp. 498–507, 2014.

[18] Z. Wang, Z. He, Z. Wang, and M. Ning, "Microwave deicing of functional pavement using sintered magnetically separated fly ash as microwave-heating aggregate," *Journal of Materials in Civil Engineering*, vol. 31, no. 7, Article ID 04019127, 2019.

[19] M. Z. Wang and F. He, *The Manufacture, Properties and Applications of Carbon Fibers*, Science Press, Beijing, 1984.

[20] D. D. L. Chung, "Cement reinforced with short carbon fibers: A multifunctional material," *Composites Part B*, vol. 31, no. 6, pp. 511–526, 2000.

[21] J. Y. Xu, D. H. Zhao, and X. Luo, *Fiber-reinforced Geopolymer Materials and Their Dynamic Mechanical Properties*, pp. 1–3, Northwestern Polytechnical University Press, Xi'an, China, 2015.

[22] J. Gao, H. Guo, X. Wang et al., "Microwave deicing for asphalt mixture containing steel wool fibers," *Journal of Cleaner Production*, vol. 206, pp. 1110–1122, 2019.

[23] B. Wang, K. Z. Li, H. J. Li, D. S. Hou, and M. Huang, "Wave absorption properties of carbon fiber reinforced cement matrix composites," *Functional Materials*, vol. 05, pp. 756–759, 2007.

[24] J. Gao, Z. W. Zhang, Z. Q. Han, A. M. Sha, and Z. J. Wang, "Research progress of electromagnetic wave absorbing materials for microwave ice and snow melting pavement," *Materials Guide*, vol. 30, no. 23, pp. 87–95, 2016.

[25] J. Gao, A. Sha, Z. Wang, Z. Tong, and Z. Liu, "Utilization of steel slag as aggregate in asphalt mixtures for microwave deicing," *Journal of Cleaner Production*, vol. 152, pp. 429–442, 2017.

[26] Z. Wang, P. Zhao, T. Ai, G. Yang, and Q. Wang, "Microwave absorbing characteristics of asphalt mixes with carbonyl iron powder," *Progress In Electromagnetics Research M*, vol. 19, pp. 197–208, 2011.

[27] C. Wang, B. Yang, G. Tan, X. Guo, L. Zhou, and S. Xiong, "Numerical analysis on thermal characteristics and ice melting efficiency for microwave deicing vehicle," *Modern Physics Letters B*, vol. 30, no. 13, Article ID 1650203, 2016.

[28] H. Chen, J. Xu, Y. Wu, J Liu, and H Huang, "Study on the thermodynamic properties of concrete surface during microwave deicing of airport pavement," *Materials*, vol. 13, no. 16, p. 3557, 2020.

[29] E. X. Feng, *Electromagnetic fields and Electromagnetic Waves*, p. 57, Xi'an Jiaotong University Press, Xi'an, China, 2010.

[30] Z. B. Zhang and R. Q. Zhong, *Fundamentals of Microwave Heating Technology*, pp. 5–80, Electronic Industry Press, Beijing, China, 1988.

[31] H. An, "Interaction of dielectric polarization and electric field," *Physics and Engineering*, vol. 13, no. 6, 2007.

[32] S. M. Ding, "Research on the key technology of electromagnetic wave-absorbing concrete materials," Dissertation, Xi'an University of Electronic Science and Technology, Xi'an, China, 2010.

[33] C. Y. Zuo and Y. M. Ding, "Research on the loss mechanism of water on microwave field," *Instrumentation Technology and Sensors*, vol. 12, pp. 61-62, 2004.